

*Full Length Research Paper*

# Nano theoretical studies of fMet-tRNA structure in protein synthesis of prokaryotes and its comparison with the structure of fAla-tRNA

F. Mollaamin\*, M. Noei, M. Monajjemi and R. Rasoolzadeh

Department of Chemistry, Science and Research Branch, Islamic Azad University, Tehran, Iran.

Accepted 15 January, 2019

In this paper, we performed quantum mechanic calculations on structures of fMet-tRNA and fAla-tRNA. Comparing the results structure design was done by formalizing the amino acid and attaching in to the adenine nucleotide of tRNA. The performed calculations are Opt, SCRF, NBO and NMR.

**Key words:** Natural bond orbital (NBO), fMet-tRNA, NMR, Opt, SCRF, fAla-tRNA.

## INTRODUCTION

It is generally accepted that initiation of protein synthesis in *Escherichia coli* starts with formyl-methionine, directed by the codons AUG or GUG. Protein synthesis proceeds by transfer of the growing polypeptide chain from the tRNA bound to the ribosomal P site to the incoming aminoacyl-tRNA in the adjacent A site. After translocation of the ribosome in the 30 direction of the mRNA, by the action of elongation factor G, the A site again becomes empty and the next codon exposed so that a new aminoacyl-tRNA ternary complex can be selected (Ogle and Ramakrishnan, 2005).

Synthetic polynucleotide containing AUG and/or GUG codons as well as natural mRNA have been used extensively in order to elucidate the mechanism of initiation of protein synthesis (Grunberg-Manago, 1977).

In all these studies it has been assumed that binding of fMet-tRNA to ribosome's is the polynucleotide in bacteria the start codon AUG is recognized by fMet-tRNA. This tRNA does not recognize internal AUG codons. Initiation of protein biosynthesis requires the correct positioning of charged initiator tRNA, fMet-tRNA in the ribosomal P-site of the mRNA-programmed 70S ribosome's (Gualerzi and Pon, 1990; La Teana et al., 1996; Monajjemi et al., 2008; Spurio et al., 1993; Forster et al., 1999).

The rapid development of molecular biology in recent years has been mirrored by the rapid development of

computer hardware and software. This improvement led to the development of sophisticated computational techniques and a wide range of computer simulations involving such methods among the areas It is well observed that fMet-tRNA is the pharmacological targets of many of the drugs that are currently in clinical use or in advanced clinical trials. Therefore, the implication throughout this paper has been profound is the modeling of fMet-tRNA structure and function, the chemical behavior of fMet-tRNA within drug design and also understanding at a molecular level of the role of solvents in biotechnological applications (Agris et al., 1997; Monajjemi et al., 2010). We selected adenine of tRNA structure (first nucleotide in acceptor arm of tRNA structure) and then perform modeling of fMet-tRNA, during the process we formylized alanine and then attached it to the adenine of tRNA and then designed the structure of fAla-tRNA to compare it with fMet-tRNA, (Figure 1).

## METHODOLOGY

At first, we have modeled the structure of fMet-tRNA and fAla-tRNA with Chem office package and then optimized at the B3LYP and HF levels of theory with 3-21G\* basis set. After fully optimization of those structures, we have calculated NMR parameters and NBO analysis at the levels of HF/3-21G\* and B3LYP/3-21G\* theory and theoretically explored the solvent effects (GAS, DMSO, CHCl<sub>3</sub>, H<sub>2</sub>O) on structure of adenine + fMet and adenine + fAla and calculations of NMR parameters and NBO calculation have been Performed on a Pentium-4 based system using GAUSSIAN

\*Corresponding author. E-mail: [smollaamin@gmail.com](mailto:smollaamin@gmail.com).

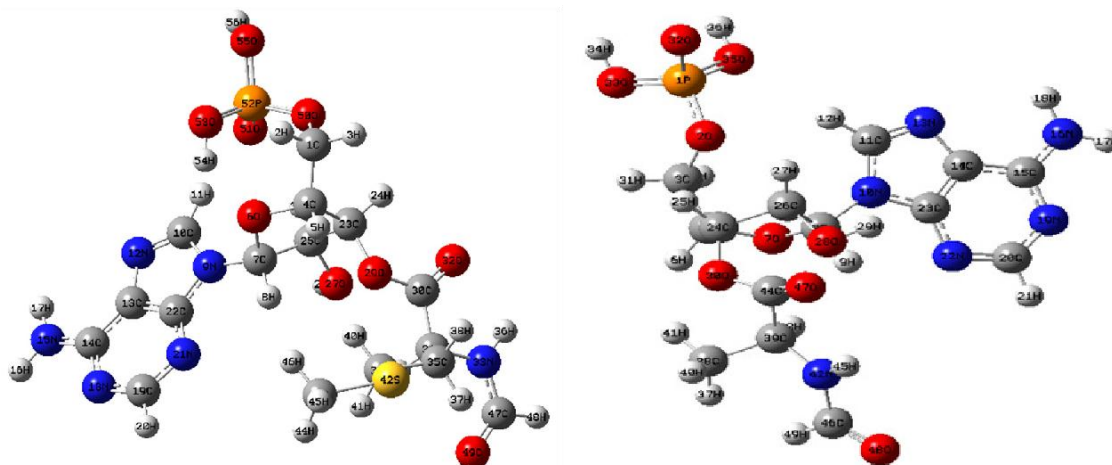


**Figure 1.** Structure of Adenine + fMet of fMet-tRNA and Adenine + fAla of fAla-tRNA

**Table 1.** Optimization energy for each method.

3-21G*	E(kcal/mol)			
	Gas	CHCL <sub>3</sub>	DMSO	H <sub>2</sub> O
HF(fMet-tRNA)	-3738.1213366	-3738.1244432	-3738.1213031	-3738.1213011
B3LYP(fMet-tRNA)	-3755.0439622	-3755.0463986	-3755.0438037	-3755.0438020
HF(fAla-tRNA)	-1174948.9244	-1174951.5084	-1174952.5478	-1174952.6039
B3LYP(fAla-tRNA)	-1180837.1055	-1180839.6468	-1180840.7420	-1180840.8019

03 program (Gaussian et al., 1998).

## RESULTS AND DISCUSSION

In this paper we performed quantum calculations on the structure of fMet-tRNA and fAla-tRNA and to perform the action, first we formalized (gave a formyl molecule to the structure) two amino acids methionine and alanine and then we attached them from tRNA to adenine nucleotide and then we performed the quantum calculations on the achieved structures (fMet-tRNA and fAla-tRNA).

In this paper HF and DFT/B3LYP methods with 3-21G\* basis set were employed for investigating the structure optimization and energy minimization of fMet-tRNA and fAla-tRNA (Figure 1) have been summarized in Table 1. The HF and DFT energies are of particular interest because they provide results for interactions appearing in solvent medium considered in this letter, which are in accord with biological behavior of fMet-tRNA and fAla-tRNA. Furthermore, recent papers often tend to ask about the role of water solvent effect on the stability of fMet-tRNA and fAla-tRNA structures. The detailed results of relative energy values for those structures in gas, DMSO, CHCL<sub>3</sub> and water solvents optimized at the HF and B3LYP levels of theory with 3-21G\* basis set are summarized in Table 1.

In the NBO analysis, in order to compute the span of the valence space, each valence bonding NBO ( $\sigma_{AB}$ ), must in turn, be paired with a corresponding valence anti bonding NBO ( $\sigma_{AB}^*$ ): Namely, the Lewis  $\sigma$ -type (donor)

NBO are complemented by the non-Lewis  $\sigma^*$ -type (acceptor) NBO that are formally empty in an idealized Lewis structure picture. Readily, the general transformation to NBO leads to orbitals that are unoccupied in the formal Lewis structure. As a result, the filled NBO of the natural Lewis structure are well adapted to describe covalency effects in molecules. Since the non-covalent delocalization effects are associated with  $\sigma \rightarrow \sigma^*$  interactions between filled (donor) and unfilled (acceptor) orbitals, it is natural to describe them as being of donor-acceptor, charge transfer, or generalized "Lewis base-Lewis acid" type. The anti bonds represent unused valence-shell capacity and spanning portions of the atomic valence space that are formally unsaturated by covalent bond formation. Weak occupancies of the valence anti bonds signal irreducible departures from an idealized localized Lewis picture, that is, true "delocalization effects". As a result, in the NBO analysis, the donor-acceptor (bond-anti bond) interactions are taken into consideration by examining all possible interactions between 'filled' (donor) Lewis-type NBO and 'empty' (acceptor) non-Lewis NBO and then estimating their energies by second-order perturbation theory.

These interactions (or energetic stabilizations) are referred to as 'delocalization' corrections to the zeroth-order natural Lewis structure. The most important interaction between "filled" (donor) Lewis-type NBO and "empty" (acceptor) non-Lewis is reported in Table 2, the level of HF/3-21G\* and B3LYP/ 3-21G\* basis set at the DFT theory. we observed interaction between Donor NBO, the LP(1,2) of O29, O32 and Acceptor NBO, the  $\sigma^*(\text{C30-O32})$ ,  $\pi^*(\text{C30 - O32})$ ,  $\sigma^*(\text{O29 - C30})$  of fMet-tRNA structure, and donor NBO, the LP(1,2) of O30, O47 and acceptor NBO, the  $\sigma^*(\text{C44-O47})$ ,  $\pi^*(\text{C44-O47})$ ,  $\sigma^*(\text{O30-C44})$  of fAla-tRNA structure and then we reported the energy and hybrid for C30-O29, C30-O32 and C30=O32 bonding of fMet-tRNA and O30-C44, C44-O47, and C44=O47 bonding of fAla-tRNA Table 3, by same level. The natural population analysis (NPA) was evaluated in terms of natural atomic orbital occupancies (Haser and Ahlrichs, 1989; Ahlrichs et al., 1989). Table 4 show the molecular charge distribution on the O29, C30 and O32 atoms in structure of fMet-tRNA and O30, C44 and O47 atoms in structure of fAla-tRNA. These partial charges distribution on the atoms shows that the electrostatic repulsion or attraction between atoms can give a significant contribution to the intra- and intermolecular interaction.

Table 5 shows calculated natural orbital occupancy (number of electron, or "natural population" of the orbital). It is noted that for  $\sigma_{\text{O29 - C30}}$  of fMet-tRNA and  $\sigma_{\text{O30-C44}}$  of fAla-tRNA bond orbital, Decreased or increased occupancy of the localized  $\sigma_{\text{O29 - C30}}$  of fMet-tRNA and  $\sigma_{\text{O30-C44}}$  of fAla-tRNA orbital in the idealized Lewis structure, and their subsequent impact on molecular stability and geometry (bond lengths) are also related with the resulting p character of the corresponding O29 natural hybrid orbital (NHO) of  $\sigma_{\text{O29 - C30}}$  and O30 natural hybrid orbital (NHO) of  $\sigma_{\text{O30-C44}}$  bond orbital.

Nuclear magnetic Resonance (NMR) is based on the quantum mechanical property of nuclei (Benas et al., 2000). The chemical shielding refers to the phenomenon which associated with the secondary magnetic field created by the induced motions of the electrons that surrounding the nuclei when in the presence of an applied magnetic field. The energy of a magnetic moment  $\mu$ , in a magnetic field, B, is as follow:

$$E = -\mu \cdot (1 - \sigma)B \quad (1)$$

Where the shielding  $\sigma$  is the differential resonance shift due to the induced motion of the electrons (Magdalena and Sadlej, 1998). In general, the electron distribution around a nucleus in a molecule is more spherically symmetric. Therefore, the size of electron current around the field, and hence the size of the shielding, will depend on the orientation of the molecule within the applied field B0 (Melinda, 2003).

For chemical shielding (CS) tensor, which describes how the size of shielding varies with molecular

orientation, we often use the following convention for the three principal components:

$$\sigma_{11} \leq \sigma_{22} \leq \sigma_{33} \quad (2)$$

The three values of the shielding tensor are frequently expressed as the isotropic value  $(\sigma_{\text{iso}})$ , the anisotropy  $(\sigma)$ , and the asymmetry  $(\eta)$ . These quantities are defined as follows [Monajjemi et al., 2004]:

1. The isotropic value  $(\sigma_{\text{ISO}})$  :

$$\sigma_{\text{ISO}} = \frac{1}{3} (\sigma_{11} + \sigma_{22} + \sigma_{33}) \quad (3)$$

2. The anisotropy shielding  $(\sigma)$  :

$$\sigma = \sigma_{33} - \frac{1}{2} (\sigma_{11} + \sigma_{22}) \quad (4)$$

3. The asymmetry parameter  $(\eta)$  :

$$\eta = \frac{|\sigma_{22} - \sigma_{11}|}{|\sigma_{33} - \sigma_{\text{ISO}}|} \quad (5)$$

Instead of deriving  $(\sigma_{\text{IND}})$  from the difference of the PCM-optimized shielding and the PCM shielding of the molecule held at the geometry optimized in vacuum, it can be obtained from the shielding calculated in vacuum for a molecule that is geometry-optimized in solution [Monajjemi et al., 2007]. Thus,

$$\sigma_{\text{IND}} = \sigma_{\text{VAC}}^{\text{SOL}}(R) - \sigma_{\text{VAC}}^{\text{REF}}(R) \quad (6)$$

Where  $\sigma_{\text{VAC}}^{\text{SOL}}(R)$  is the value of the nuclear shielding in vacuum but with the solute geometry optimized in solution  $\sigma_{\text{VAC}}^{\text{REF}}(R)$  are the corresponding parameters for calculation with reference solvent. In this case, we may suppose that optimization of solute molecule in solvent and then performing shielding calculations is similar to shielding calculations in the isolated system (Lynden and Rasaiah, 1997).

Self-Consistent Reaction Field (SCRf) method is based on a continuum model with uniform dielectric constant  $(\epsilon)$ . The simplest SCRf model is the Onsager reaction field model. In this method, the solute occupies a fixed spherical cavity of radius  $a_0$  within the solvent field. A dipole in the molecule will induce a dipole in the medium, and the electric field applied by the solvent dipole will in turn interact with the molecular dipole leading to net stabilization.

The Gauge Including Atomic Orbital (GIAO) approach

**Table 2.** Second order perturbation theory analysis of NBOHF/3-21G\* method.

Phase (fMet-tRNA)	Donor NBO (i)	Acceptor NBO (j)	E(2) (kcal/mol)	Phase (fAla-tRNA)	Donor NBO (i)	Acceptor NBO (j)	E(2) (kcal/mol)
Gas	LP ( 1) O29	$\sigma^*$ C30 - O32	9.57	Gas	LP ( 1) O30	$\sigma^*$ C44 – O47	9.83
	LP ( 2) O29	$\pi^*$ C30 - O32	60.32		LP ( 2) O30	$\pi^*$ C44 – O47	55.20
	LP ( 1) O32	$\sigma^*$ O29 - C30	0.58		LP ( 1) O47	$\sigma^*$ O30 – C44	0.78
	LP ( 2) O32	$\sigma^*$ O29 - C30	51.40		LP ( 2) O47	$\sigma^*$ O30 – C44	53.18
CHCl <sub>3</sub>	LP ( 1) O29	$\sigma^*$ C30 - O32	9.62	CHCl <sub>3</sub>	LP ( 1) O30	$\sigma^*$ C44 – O47	9.93
	LP ( 2) O29	$\pi^*$ C30 - O32	60.72		LP ( 2) O30	$\pi^*$ C44 – O47	56.26
	LP ( 1) O32	$\sigma^*$ O29 - C30	0.57		LP ( 1) O47	$\sigma^*$ O30 – C44	0.76
	LP ( 2) O32	$\sigma^*$ O29 - C30	51.15		LP ( 2) O47	$\sigma^*$ O30 – C44	52.58
DMSO	LP ( 1) O29	$\sigma^*$ C30 - O32	11.16	DMSO	LP ( 1) O30	$\sigma^*$ C44 – O47	10.00
	LP ( 2) O29	$\pi^*$ C30 - O32	70.17		LP ( 2) O30	$\pi^*$ C44 – O47	56.98
	LP ( 1) O32	$\sigma^*$ O29 - C30	1.64		LP ( 1) O47	$\sigma^*$ O30 – C44	0.74
	LP ( 2) O32	$\sigma^*$ O29 - C30	43.20		LP ( 2) O47	$\sigma^*$ O30 – C44	52.18
H <sub>2</sub> O	LP (1) O29	$\sigma^*$ C30 - O32	9.66	H <sub>2</sub> O	LP ( 1) O30	$\sigma^*$ C44 – O47	9.97
	LP (2) O29	$\pi^*$ C30 - O32	60.12		LP ( 2) O30	$\pi^*$ C44 – O47	56.66
	LP (1) O32	$\sigma^*$ O29 - C30	0.58		LP ( 1) O47	$\sigma^*$ O30 – C44	0.75
	LP (2) O32	$\sigma^*$ O29 - C30	51.56		LP ( 2) O47	$\sigma^*$ O30 – C44	52.35
<b>B3LYP/3-21G* method</b>							
Phase (fMet-tRNA)	Donor NBO (i)	Acceptor NBO (j)	E(2) (kcal/mol)	Phase (fAla-tRNA)	Donor NBO (i)	Acceptor NBO (j)	E(2) (kcal/mol)
Gas	LP ( 1) O29	$\sigma^*$ C30 - O32	7.25	Gas	LP ( 1) O30	$\sigma^*$ C44 –O47	7.06
	LP ( 2) O29	$\pi^*$ C30 - O32	55.35		LP ( 2) O30	$\pi^*$ C44 –O47	39.81
	LP ( 1) O32	$\sigma^*$ O29 - C30	0.72		LP ( 1) O47	$\sigma^*$ O30 –C44	0.75
	LP ( 2) O32	$\sigma^*$ O29 - C30	37.09		LP ( 2) O47	$\sigma^*$ O30 –C44	41.29
CHCl <sub>3</sub>	LP ( 1) O29	$\sigma^*$ C30 - O32	7.28	CHCl <sub>3</sub>	LP ( 1) O30	$\sigma^*$ C44 –O47	7.15
	LP ( 2) O29	$\pi^*$ C30 - O32	55.66		LP ( 2) O30	$\pi^*$ C44 –O47	40.70
	LP ( 1) O32	$\sigma^*$ O29 - C 30	0.71		LP ( 1) O47	$\sigma^*$ O30 –C44	0.73
	LP ( 2) O32	$\sigma^*$ O29 - C 30	36.98		LP ( 2) O47	$\sigma^*$ O30 –C44	40.68
DMSO	LP ( 1) O29	$\sigma^*$ C30 - O 32	8.34	DMSO	LP ( 1) O30	$\sigma^*$ C44 –O47	7.17
	LP ( 2) O29	$\pi^*$ C30 - O32	50.45		LP ( 2) O30	$\pi^*$ C44 –O47	40.86
	LP ( 1) O32	$\sigma^*$ O29 - C30	1.55		LP ( 1) O47	$\sigma^*$ O30 –C44	0.73
	LP ( 2) O32	$\sigma^*$ O29 - C30	37.09		LP ( 2) O47	$\sigma^*$ O30 –C44	40.57
H <sub>2</sub> O	LP ( 1) O29	$\sigma^*$ C30 - O 32	7.25	H <sub>2</sub> O	LP ( 1) O30	$\sigma^*$ C44 –O47	7.15
	LP ( 2) O29	$\pi^*$ C30 - O32	55.35		LP ( 2) O30	$\pi^*$ C44 –O47	40.67
	LP ( 1) O32	$\sigma^*$ O29 - C 30	0.72		LP ( 1) O47	$\sigma^*$ O30 –C44	0.73
	LP ( 2) O32	$\sigma^*$ O29 - C 30	37.09		LP ( 2) O47	$\sigma^*$ O30 –C44	40.70

was used. The ab initio GIAO calculations of NMR chemical shielding tensors were performed using the DFT and HF method. The chemical shielding tensors were calculated with the GAUSSIAN 03 program. The isotropic chemical shielding ( $\sigma_{iso}$ ), asymmetry parameter ( $\eta$ ) and anisotropy shielding ( $\sigma$ ) for O(29),O(32), C(30) atoms of fMet-tRNA, and O(30),C(44) and O(47) atoms in structure of fAla-tRNA (Figure 1) have been summarized in Table 6 and O(29),O(32)and C(30) atoms are

the connections of adenine of fMet and also O(30), C(44) and O(47) atoms are the connections of adenine to fAla, these atoms are so important to us.

## Conclusion

In this work, we have summarized:

1. Optimization at the HF and DFT levels of theory

**Table3.** Calculated natural hybrid orbitals (NHOs) and the polarization coefficient for each hybrid in the corresponding NBO (parentheses) for the selected fMet-tRNA (1) and fAla-tRNA (2) using the selected methods.

Phase	Bond Hybrids (1)	C <sub>30</sub> -O <sub>29</sub>	C <sub>30</sub> O <sub>29</sub>	C <sub>30</sub> -O <sub>32</sub>	C <sub>30</sub> O <sub>32</sub>	C <sub>30</sub> =O <sub>32</sub>	C <sub>30</sub> O <sub>32</sub>
Gas	HF/3-21G* B3LYP/3-21G*	sp <sup>2.66</sup> (0.5472) sp <sup>2.64</sup> (0.5602)	sp <sup>1.93</sup> (0.8370) sp <sup>2.19</sup> (0.8283)	sp <sup>2.07</sup> (0.5732) sp <sup>2.12</sup> (0.5811)	sp <sup>1.26</sup> (0.8194) sp <sup>1.56</sup> (0.8138)	sp <sup>1.00</sup> (0.5433) sp <sup>99.99</sup> (0.5660)	sp <sup>1.00</sup> (0.8396) sp <sup>99.99</sup> (0.8244)
CHCL <sub>3</sub>	HF/3-21G* B3LYP/ 3-21G*	sp <sup>2.64</sup> (0.5484) sp <sup>2.63</sup> (0.5610)	sp <sup>1.94</sup> (0.8362) sp <sup>2.20</sup> (0.8278)	sp <sup>2.07</sup> (0.5735) sp <sup>2.12</sup> (0.5815)	sp <sup>1.26</sup> (0.8192) sp <sup>1.57</sup> (0.8136)	sp <sup>1.00</sup> (0.5448) sp <sup>99.99</sup> (0.5673)	sp <sup>1.00</sup> (0.8385) sp <sup>99.99</sup> (0.8235)
DMSO	HF/3-21G* B3LYP/3-21G*	sp <sup>2.66</sup> (0.5472) sp <sup>2.66</sup> (0.5472)	sp <sup>1.93</sup> (0.8370) sp <sup>1.93</sup> (0.8370)	sp <sup>2.07</sup> (0.5735) sp <sup>2.07</sup> (0.5732)	sp <sup>1.26</sup> (0.8192) sp <sup>1.26</sup> (0.8194)	sp <sup>1.00</sup> (0.5433) sp <sup>99.99</sup> (0.5660)	sp <sup>1.00</sup> (0.8396) sp <sup>99.99</sup> (0.8244)
H <sub>2</sub> O	HF/3-21G* B3LYP/3-21G*	sp <sup>2.66</sup> (0.5472) sp <sup>2.64</sup> (0.5602)	sp <sup>1.93</sup> (0.8370) sp <sup>2.19</sup> (0.8283)	sp <sup>2.08</sup> (0.5729) sp <sup>2.12</sup> (0.5811)	sp <sup>1.26</sup> (0.8196) sp <sup>1.56</sup> (0.8138)	sp <sup>1.00</sup> (0.5439) sp <sup>99.99</sup> (0.5660)	sp <sup>1.00</sup> (0.8392) sp <sup>99.99</sup> (0.8394)
Phase	Bond Hybrids(2)	O <sub>30</sub> - C <sub>44</sub>	O <sub>30</sub> C <sub>44</sub>	C <sub>44</sub> - O <sub>47</sub>	C <sub>44</sub> O <sub>47</sub>	C <sub>44</sub> =O <sub>47</sub>	C <sub>44</sub> O <sub>47</sub>
Gas	HF/3-21G* B3LYP/3-21G*	sp <sup>1.99</sup> (0.8363) sp <sup>2.40</sup> (0.8277)	sp <sup>2.67</sup> (0.5482) sp <sup>2.70</sup> (0.5611)	sp <sup>2.04</sup> (0.5730) sp <sup>2.05</sup> (0.5794)	sp <sup>1.24</sup> (0.8196) sp <sup>1.46</sup> (0.8151)	sp <sup>1.00</sup> (0.5506) sp <sup>99.99</sup> (0.5821)	sp <sup>1.00</sup> (0.8348) sp <sup>99.99</sup> (0.8131)
CHCL <sub>3</sub>	HF/3-21G* B3LYP/ 3-21G*	sp <sup>2.02</sup> (0.8351) sp <sup>2.44</sup> (0.8262)	sp <sup>2.64</sup> (0.5501) sp <sup>2.67</sup> (0.5634)	sp <sup>2.04</sup> (0.5728) sp <sup>2.05</sup> (0.5792)	sp <sup>1.24</sup> (0.8197) sp <sup>1.45</sup> (0.8152)	sp <sup>1.00</sup> (0.5489) sp <sup>99.99</sup> (0.5806)	sp <sup>1.00</sup> (0.8359) sp <sup>99.99</sup> (0.8142)
DMSO	HF/3-21G* B3LYP/3-21G*	sp <sup>2.03</sup> (0.8343) sp <sup>2.45</sup> (0.8259)	sp <sup>2.63</sup> (0.5514) sp <sup>2.66</sup> (0.5638)	sp <sup>2.04</sup> (0.5726) sp <sup>2.05</sup> (0.5791)	sp <sup>1.23</sup> (0.8198) sp <sup>1.45</sup> (0.8152)	sp <sup>1.00</sup> (0.5478) sp <sup>99.99</sup> (0.5804)	sp <sup>1.00</sup> (0.8366) sp <sup>99.99</sup> (0.8144)
H <sub>2</sub> O	HF/3-21G* B3LYP/3-21G*	sp <sup>2.03</sup> (0.8346) sp <sup>2.44</sup> (0.8263)	sp <sup>2.63</sup> (0.5508) sp <sup>2.67</sup> (0.5633)	sp <sup>2.04</sup> (0.5727) sp <sup>2.05</sup> (0.5792)	sp <sup>1.24</sup> (0.8198) sp <sup>1.45</sup> (0.8152)	sp <sup>1.00</sup> (0.5483) sp <sup>99.99</sup> (0.5807)	sp <sup>1.00</sup> (0.8363) sp <sup>99.99</sup> (0.8141)

provides a suitable computational model in terms of calculated NMR parameters and relative energies.

2. There was an increase in the relative stability of the interested structures through the improvement of basis set and including electron correlations, Hence, the most stable structures are perceived in the CHCL<sub>3</sub> solution at the B3LYP/3-21G\* level of theory.

3. We observed an increase in values of NMR chemical shielding around O<sub>29</sub>, O<sub>32</sub> By increasing lone pair electrons contribution of oxygen (O<sub>29</sub>, O<sub>32</sub>) atoms in resonance Interactions, Hence, O<sub>29</sub> atom has the highest chemical shielding among the oxygen atoms (fMet-tRNA).

4. We observed a decrease in the bond lengths of the O<sub>29</sub>-C<sub>30</sub> of the structure by the increase of

solvent dielectric constant (fMet-tRNA).

5. We observed an increase in the relative stability by increasing the LP Os (O<sub>29</sub>, O<sub>32</sub>) electrons contribution in the enhancement of π electron clouds (fMet-tRNA).

6. In many lab experiments it is proven that the real structure to start protein synthesis in prokaryotes is fMet-tRNA and we studied calculated and worked out the stability and the

**Table 4.** Atomic charge distribution described in terms of natural population analysis (NPA) for the compounds studied.

<b>fMet-tRNA</b>		<b>Gas</b>	<b>CHCL<sub>3</sub></b>	<b>DMSO</b>	<b>H<sub>2</sub>O</b>
O29	HF/3-21G*	-0.63608	-0.63768	-0.63608	-0.71482
	B3LYP/3-21G*	-0.49088	-0.49162	-0.49088	-0.5048
C30	HF/3-21G*	0.94389	0.94185	0.94389	0.981579
	B3LYP/3-21G*	0.75659	0.75427	0.75659	0.732509
O32	HF/3-21G*	-0.6402	-0.63594	-0.64019	-0.62108
	B3LYP/3-21G*	-0.55198	-0.54844	-0.55197	-0.51221
<b>fAla-tRNA</b>		<b>GAS</b>	<b>CHCl<sub>3</sub></b>	<b>DMSO</b>	<b>H<sub>2</sub>O</b>
O30	HF/3-21G*	-0.64032	-0.63862	-0.63746	-0.63797
	B3LYP/3-21G*	-0.51736	-0.51386	-0.5132	-0.514
C44	HF/3-21G*	0.94048	0.94202	0.94294	0.94255
	B3LYP/3-21G*	0.75557	0.75507	0.75491	0.7551
O47	HF/3-21G*	-0.62227	-0.62765	-0.63107	-0.6296
	B3LYP/3-21G*	-0.50732	-0.51388	-0.51502	-0.51364

**Table 5.** Occupancy and Energy (kcal/mol) for between O29 - C30 atoms of -tRNA and  $\sigma$  O30-C44 of fAla-tRNA.

<b>Phase</b>	<b>Method</b>	<b>NBO</b>	<b>Occupancy</b>	<b>Energy(kcal/mol)</b>
Gas	HF/3-21G*	$\sigma$ O29 - C30	1.99398	-773.7261
	B3LYP/3-21G*	$\sigma$ O29 - C30	1.99305	-605.5910
CHCL <sub>3</sub>	HF/3-21G*	$\sigma$ O29 - C30	1.99399	-774.9309
	B3LYP/3-21G*	$\sigma$ O29 - C30	1.99308	-606.6076
DMSO	HF/3-21G*	$\sigma$ O29 - C30	1.99397	-773.5423
	B3LYP/3-21G*	$\sigma$ O29 - C30	1.99305	-605.5910
H <sub>2</sub> O	HF/3-21G*	$\sigma$ O29 - C30	1.99395	-773.3433
	B3LYP/3-21G*	$\sigma$ O29 - C30	1.99305	-605.5910
<b>Phase</b>	<b>Method</b>	<b>NBO</b>	<b>Occupancy</b>	<b>Energy (kcal/mol)</b>
Gas	HF/3-21G*	$\sigma$ O30 - C44	1.99342	-760.8998
	B3LYP/3-21G*	$\sigma$ O30 - C44	1.9909	-568.1538
CHCL <sub>3</sub>	HF/3-21G*	$\sigma$ O30 - C44	1.99343	-764.6523
	B3LYP/3-21G*	$\sigma$ O30 - C44	1.991	-574.0712
DMSO	HF/3-21G*	$\sigma$ O30 - C44	1.99343	-767.2251
	B3LYP/3-21G*	$\sigma$ O30 - C44	1.99102	-575.2008
H <sub>2</sub> O	HF/3-21G*	$\sigma$ O30 - C44	1.99343	-766.1019
	B3LYP/3-21G*	$\sigma$ O30 - C44	1.991	-573.8453

real reasons that why this structure is produced in protein synthesis in prokaryotes and fAla-tRNA is not produced there and presented the results and finding in the charts.

As O(29), O(32) and C(30) atoms are the connections of adenine of fMet and also O(30), C(44) and O(47) atoms are the connections of adenine to fAla, these atoms are

**Table 6.** NMR parameters (ppm) of O(29) and C(30) and O(32) atoms of fMet-tRNA and O(30), C(44) and O(47) atoms of fAla-tRNA structures in gas phase at the level of HF/3-21G\* and B3LYP/3-21G\* theory.

<b>NMR parameters</b>	<b>GAS</b>
HF/3-21G* O(29) $\sigma_{ISO}$	221.0980
HF/3-21G* O(29) $\sigma$	229.6773
HF/3-21G* O(29) $\eta$	-1.7280
B3LYP/3-21G*O(29) $\sigma_{ISO}$	137.0772
B3LYP/3-21G* O(29) $\sigma$	148.2147
B3LYP/3-21G* O(29) $\eta$	-0.7952
HF/3-21G* C(30) $\sigma_{ISO}$	44.2825
HF/3-21G* C(30) $\sigma$	94.7091
HF/3-21G* C(30) $\eta$	14.5365
B3LYP/3-21G* C(30) $\sigma_{ISO}$	36.1343
B3LYP/3-21G* C(30) $\sigma$	57.9762
B3LYP/3-21G* C(30) $\eta$	16.9674
HF/3-21G*O(32) $\sigma_{ISO}$	-50.7765
HF/3-21G* O(32) $\sigma$	-52.6285
HF/3-21G* O(32) $\eta$	-1.6899
B3LYP/3-21G* O(32) $\sigma_{ISO}$	-46.0160
B3LYP/3-21G* O(32) $\sigma$	-200.8172
B3LYP/3-21G* O(32) $\eta$	-0.5470
<b>NMR parameters</b>	<b>GAS</b>
HF/3-21G* O(30) $\sigma_{ISO}$	225.4508
HF/3-21G* O(30) $\sigma$	162.0936
HF/3-21G* O(30) $\eta$	0.3047
B3LYP/3-21G*O(30) $\sigma_{ISO}$	159.0905
B3LYP/3-21G* O(30) $\sigma$	96.9107
B3LYP/3-21G* O(30) $\eta$	-0.1120
HF/3-21G* C(44) $\sigma_{ISO}$	46.3914
HF/3-21G* C(44) $\sigma$	23.04415
HF/3-21G* C(44) $\eta$	2.9532
B3LYP/3-21G* C(44) $\sigma_{ISO}$	39.8319
B3LYP/3-21G* C(44) $\sigma$	113.81215
B3LYP/3-21G* C(44) $\eta$	2.3026
HF/3-21G*O(47) $\sigma_{ISO}$	-63.6974
HF/3-21G* O(47) $\sigma$	-104.9796
HF/3-21G* O(47) $\eta$	-1.6079
B3LYP/3-21G* O(47) $\sigma_{ISO}$	-69.3989
B3LYP/3-21G* O(47) $\sigma$	-138.4288
B3LYP/3-21G* O(47) $\eta$	-1.3863

so important to us.

7. The largest  $\rho_{iso}$  value of mentioned nuclei of Adenine+fMet of fMet-tRNA structure observed for O(29), whereas the smallest one belongs to O(32). It is interesting to note that the opposite trend have been observed for asymmetry parameters  $\eta$ . This usual behavior may be readily understood in accord with biotechnological conceptions.

## REFERENCES

- Agris PF, Guenther R, Ingram PC, Basti MM, Stuart JW, Sochacka E, Malkiewicz A (1997). Unconventional structure of tRNA(Lys)SUU anticodon explains tRNA's role in bacterial and mammalian ribosomal frameshifting and primer selection by HIV. RNA., 20: 420-428.
- Ahlrichs R, Barr M, Haser M, Horn H (1989). Electronic structure calculation on workstation computers: The program system TUBBOMOLE. Komel, Chem. Phys. Lett., 162: 55- 65.
- Forster C, Krait C, Welfe H, Gualerzi, CO, Heinemann U (1999). Preliminary characterization by X-ray diffraction and Raman spectroscopy of a crystalline complex of *Bacillus stearothermophilus* initiation factor 2C-domain and (fMet). Acta Crystallogr., D55: 712-216.
- Gaussian, Revision A, Frisch MJ, Trucks GW, Schlegel HB, Scuseria GE, Grunberg-Manago M (1977). Initiation mechanisms of protein syntethesis. Prog. Nuel. Acid Res. Mol. Biol., 20: 209-284.
- Gualerzi CO, Pon CL (1990). Initiation of messenger-RNA translation in prokaryotes. Biochemistry, 29: 5881-5889.
- Haser M, Ahlrichs R (1989). Improvements on the direct SCF method. J. Comput. Chem., 10: 98- 104.
- La Teana A, Pon CL, Gualerzi CO (1996). Translation of mRNAs with degenerate initiation triplet AUU displays high initiation factor 2 dependence and is subject to initiation factor 3 repression. J. Mol. Biol., 256: 667-675.
- Lynden Bell RM, Rasaiah JC (1997). Mobility and Solvation of Ions in Channels. J. Chem. Phys., 107: 1981-1991.
- Magdalena P, Sadlej J (1998). Solvent effects on NMR spectrum of acetylene calculated by *ab initio* methods Chemical physics. Chem Phys., 234: 111-119.
- Melinda AJD (2003). Solid state NMR spectroscopy; Principles and Applications, Cambridge press, 23: 125-137.
- Monajjemi M, Heshmat M, Aghaei H, Ahmadi R, Zare K (2007). Solvent Effect on 14N NMR Shielding of Glycine, Serine, Leucine, and Threonine: Comparison Between Chemical Shifts And Energy Versus Dielectric Constant. Bull. Chem. Soc. Ethiop., 21: 111-116.
- Monajjemi M, Razavian MH, Mollaamin F, Naderi F, Honarparvar B (2008). A Theoretical thermochemical study of solute-solvent dielectric effects in the displacement of codon-anticodon base pairs. Russian J. Physical Chem. A., 82: 2277-2285.
- Monajjemi M, Noei M, Mollaamin F (2010). Design of fMet-tRNA and Calculation of its Bonding Properties by Quantum Mechanics. Nucleosides, Nucleosides Nucleotides Nucleic Acids, 29: 676-683.
- Monajjemi M, Ghiasi R, Ketabi S (2004). A theoretical study of metal-stabilised rare tautomers stability: N4 metalated cytosine (M=Be<sup>2+</sup>, Mg<sup>2+</sup>, Ca<sup>2+</sup>, Sr<sup>2+</sup> and Ba<sup>2+</sup>) in gas phase and different solvents, J. Chem. Res., 1: 11-18.
- Ogle JM, Ramakrishnan V (2005). Structural insights into translational fidelity. Ann. Rev. Biochem., 74: 129-177.
- Spurio R, Severini M, La Teana A, Canonaco MA, Pawlik RT, Gualerzi CO, Pon CL (1993). The Translational Apparatus: Structure, unction, Regulation, Evolution. Plenum Press, New York, 34: 241-252.